Journal Article

Comparative study of the accuracy of the PSM and Kogelnik models of diffraction in reflection and transmission holographic gratings

Brotherton-Ratcliffe, D., Shi, L., Osanlou, A. and Excell, P.

A Comparative Study of the Accuracy of the PSM and Kogelnik Models of Diffraction in Reflection and Transmission Holographic Gratings

D.Brotherton-Ratcliffe[1,2*], Lishen Shi[1], Ardie Osanlou[1] and Peter Excell[1]

[1]*Centre for Applied Photonics, Applied Science, Computing and Engineering, Glyndŵr University, Mold Road, Wrexham, Wales, LL11 2AW, UK*

[2]*Geola Technologies Ltd, Sussex Innovation Centre, Science Park Square, Falmer, East Sussex, BN1 9SB, UK*

dbr@geola.co.uk

Abstract: Calculated diffractive efficiencies in the visible spectral band from lossless planar holographic gratings are studied using the PSM and Kogelnik models of diffraction for the case of the σ-polarization. The results are numerically compared with rigorous coupled wave calculations over a wide parameter space covering both transmission and reflection geometries. For most reflection gratings, the PSM model is shown to consistently provide a marginally superior estimation of the diffractive efficiency. This is particularly evident in a clearly superior description of the diffractive sideband structure for most gratings, both in terms of angle and wavelength. For the transmission grating, the PSM model continues to provide a relatively good description of diffraction at low permittivity modulations and lower incidence angles with respect to the grating plane normal. However, overall Kogelnik's theory is shown to provide a somewhat superior estimation of diffractive efficiency and a clearly superior description of the diffractive side-band structure in the transmission case.

OCIS codes: (090.0090) Holography; (050.1960) Diffraction Theory.

References and links

1. D.Brotherton-Ratcliffe, "A treatment of the general volume holographic grating as an array of parallel stacked mirrors," J. Mod Optic. **59**, 1113-1132 (2012).
2. D.Brotherton-Ratcliffe, "Analytical treatment of the polychromatic spatially multiplexed volume holographic grating," Appl. Opt. **51**, 7188-7199 (2012).
3. D.Brotherton-Ratcliffe, "A new type of coupled wave theory capable of analytically describing diffraction in polychromatic spatially multiplexed holographic gratings," Journal of Physics: Conference Series **415** (2013) 012034 doi:10.1088/1742-6596/415/1/012034.
4. H.Bjelkhagen and D.Brotherton-Ratcliffe , "Ultra-realistic Imaging – advanced techniques in analogue and digital colour holography", Book, 638 pages, full colour, Taylor and Francis□ISBN-10: 1439827990 | ISBN-13: 978-1439827994, (2012).
5. M.P.Rouard, "Etudes des propriétés optiques des lames métalliques très minces," Ann. Phys. (Paris) Ser. II **7**, 291-384 (1837).
6. F.Abeles, "Recherches sur la propagation des ondes électromagnétiques sinusoïdales dans les milieux stratifiés, Application aux couches minces," Ann. Phys. (Paris) **5**, 596-640 (1950).
7. M.G.Moharam and T.K.Gaylord, "Chain-matrix analysis of arbitrary-thickness dielectric reflection gratings," J. Opt. Soc. Am. **72**, 187-190 (1982).
8. O.S.Heavens, "Optical Properties of thin films," Reports on Progress in Physics, Vol XXIII, (1960) p1.
9. H.Kogelnik, "Coupled wave theory for thick hologram gratings," Bell Syst. Tech. J. **48**, 2909-2947 (1969).
10. M.G.Moharam and T.K.Gaylord, "Rigorous coupled wave analysis of planar grating diffraction," J. Opt. Soc. Am. **71**, 811-818 (1981).
11. J.A.Kong, "Second order coupled mode equations for spatially periodic media," J. Opt. Soc. Am. **67**, 825-9 (1977).

1. Introduction

The Parallel Stacked Mirror (PSM) model[1-4] of diffraction from planar gratings provides a pleasingly intuitive model of the diffraction process occurring within the grating. The model is based on an application of the concept of Fresnel reflection as first suggested by Rouard in 1937[5].

In the PSM model, the grating is decomposed into an infinite series of parallel stacked mirrors, each possessing an infinitesimal thickness; at each mirror the classical laws of Fresnel transmission and reflection are applied. In this way a reference wave, which illuminates the grating, provokes an infinite sum of secondary "Fresnel" waves, which add to form the diffractive response.

The PSM model can also be viewed as a type of differential generalization of the chain matrix method, which is often used in the numerical calculation of the optical properties of stratified media[6-8].

Kogelnik's coupled wave model[9] of diffraction from planar gratings predated the PSM model by over 40 years. Unarguably it has provided an enormously useful model of diffraction from the simple planar grating. Like the PSM model it makes use of only two waves – a reference or illuminating wave and a provoked signal wave.

Because both the PSM and Kogelnik theories are coupled wave theories making use of only two waves, both theories are intrinsically approximate. An exception is the case of the normal incidence unslanted lossless reflection phase grating where the principle two-wave equations of the PSM theory are actually an exact analytical solution of Maxwell's equations.

In contrast to the "approximate" theories of Kogelnik and PSM, Rigorous Coupled Wave theory[10] (RCW) provides a method of describing the diffractive process to any accuracy required. The theory makes use of a potentially infinite number of coupled waves. The number of waves retained in a calculation depends on the accuracy required, a proportion of which will be evanescent waves. From a practical point of view RCW theory is a numerical technique requiring the solution either of a set of differential equations or the determination of the eigenvalues of a large matrix. As such it cannot offer the advantages of the simple analytic expressions inherent to both Kogelnik's theory and the PSM model.

In the present work we compare the predictions of Kogelnik's theory and the PSM theory with numerical RCW calculations, for both transmission and reflection gratings, in order to identify which analytic theory should best be used and under what circumstances.

2. PSM and Kogelnik Models

Fig.1 shows a simple lossless tilted planar phase grating with illuminating reference wave of amplitude R and provoked signal wave of amplitude S. Depending on the tilt angle, ψ the diagram can represent a reflection or transmission grating. Both the PSM and Kogelnik models, which model the process of diffraction within the grating, can be written in terms of the same differential equations[1,4] which are valid for the σ-polarization.

$$c_R \frac{dR}{dy} = -i\kappa S$$
$$c_S \frac{dS}{dy} = -i\vartheta S - i\kappa R \qquad (1)$$

The coefficients of these equations are different for the PSM and Kogelnik models. For the Kogelnik model,

$$c_{R(KOG)} = \cos(\theta_c - \psi)$$
$$c_{S(KOG)} = \cos(\theta_c - \psi) - 2\alpha \cos\theta_r \cos\psi \qquad (2)$$
$$\vartheta_{(KOG)} = 2\alpha\beta \cos\theta_r (\cos\theta_c - \alpha \cos\theta_r)$$

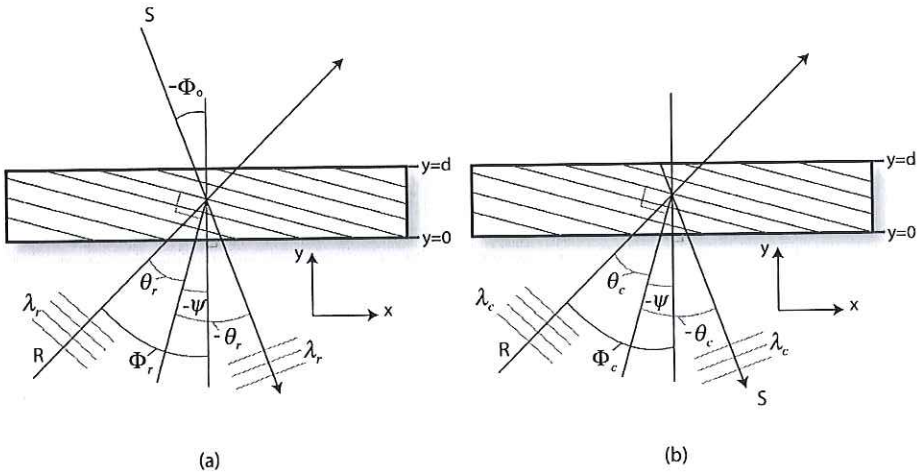

Fig.1 Holographic recording (a) and replay (b) of a simple planar grating. Note that the effect of Snell's law has not been explicitly displayed in the diagram. As such all incidence angles shown here are "internal" angles.

whereas for the PSM model,

$$c_{R(PSM)} = \frac{\cos\theta_c \cos(\theta_c - \psi)}{\alpha \cos\theta_r}$$

$$c_{S(PSM)} = \frac{-\cos\theta_c \cos(\theta_c + \psi)}{\alpha \cos\theta_r} \tag{3}$$

$$\vartheta_{(PSM)} = 2\beta(1 - \frac{\cos\theta_c}{\alpha \cos\theta_r})\cos^2\theta_c$$

Here α represents the ratio of replay to recording wavelength,

$$\alpha = \lambda_c / \lambda_r \tag{4}$$

β is the propagation constant defined as

$$\beta = \frac{2\pi n_0}{\lambda_c} \tag{5}$$

and κ is Kogelnik's coupling coefficient,

$$\kappa = \frac{\pi n_1}{\lambda_c} . \tag{6}$$

In the PSM model the recording scenario of Fig.1(a) is assumed to lead to a sinusoidal grating of the following refractive index profile

$$n = n_0 + \frac{n_1}{2}\left\{e^{i\mathbf{K}\cdot\mathbf{r}} + e^{-i\mathbf{K}\cdot\mathbf{r}}\right\} \tag{7}$$

where **K** is the grating vector. In Kogelnik's theory, as with rigorous coupled wave theory, it is the permittivity profile which must be assumed to be harmonic

$$\varepsilon = \varepsilon_0 + \frac{\varepsilon_1}{2}\left\{e^{i\mathbf{K}\cdot\mathbf{r}} + e^{-i\mathbf{K}\cdot\mathbf{r}}\right\} . \tag{8}$$

For small index therefore, both PSM and Kogelnik's theory accurately describe the same harmonic grating. However as we shall discuss later, for larger index modulations we must

make allowance for the fact that the PSM model describes a harmonic index grating rather than a harmonic permittivity grating.

Equations (1) can be solved analytically for boundary conditions corresponding either to reflection gratings or transmission gratings.

2.1 Reflection Grating

In the case of a reflection grating the appropriate boundary conditions are[1,4]

$$R(0) = 1 \qquad S(d) = 0 \tag{9}$$

The diffractive efficiency of the grating may then be written as

$$\eta_\sigma = \frac{|c_s|}{c_R} S(0)S^*(0) = \frac{\kappa^2 \sinh^2(d\Upsilon)}{\kappa^2 \sinh^2(d\Upsilon) - c_R c_S \Upsilon^2} \tag{10}$$

where

$$\Upsilon^2 = -\frac{\vartheta^2}{4c_S^2} - \frac{\kappa^2}{c_R c_S} \tag{11}$$

Substitution of equations (2) or (3) into these formulae defines respectively either the Kogelnik prediction or the PSM prediction of diffractive efficiency.

2.2 Transmission Grating

In the case of a transmission grating the boundary conditions are

$$R(0) = 1 \qquad S(0) = 0 \tag{12}$$

The diffractive efficiency of the grating may then be written as

$$\eta_\sigma = \frac{\kappa^2}{2\Upsilon^2 c_S c_R} \{\cosh(2d\Upsilon) - 1\} \tag{13}$$

where Υ is given by equation (11).

Once again, substitution of equations (2) or (3) into these formulae defines respectively either the Kogelnik prediction or the PSM prediction of diffractive efficiency. It should be noted that for the special case of Bragg resonance the Kogelnik and PSM models reduce to the same analytic expressions for diffraction efficiency for either transmission or reflection gratings[1,4].

3. Comparison with RCW Calculations

In the following sections we will describe the results of a systematic comparison of the analytic formulae given above with accurate numerical calculations using RCW theory for the harmonic permittivity case. The numerical RCW algorithm that we have used for this purpose is described in the appendix. Note that as pointed out before, PSM is a *harmonic index theory* whereas the Kogelnik model and standard RCW theory naturally describe a *harmonic permittivity*. As we shall see, only for very high index modulations do we need to worry about this difference.

Throughout the analysis that follows we will concentrate on holographic gratings made and replayed in air. The effect of Snell's law is considerable here. For both transmission and reflection gratings it limits the replay reference beam angle within the grating to between ±40°. In the case of the reflection grating it also limits the range of possible grating tilt angles from $|\psi| = 0$ to 40°. For the transmission grating Snell's law limits the grating tilt angle to between 60° and 120°.

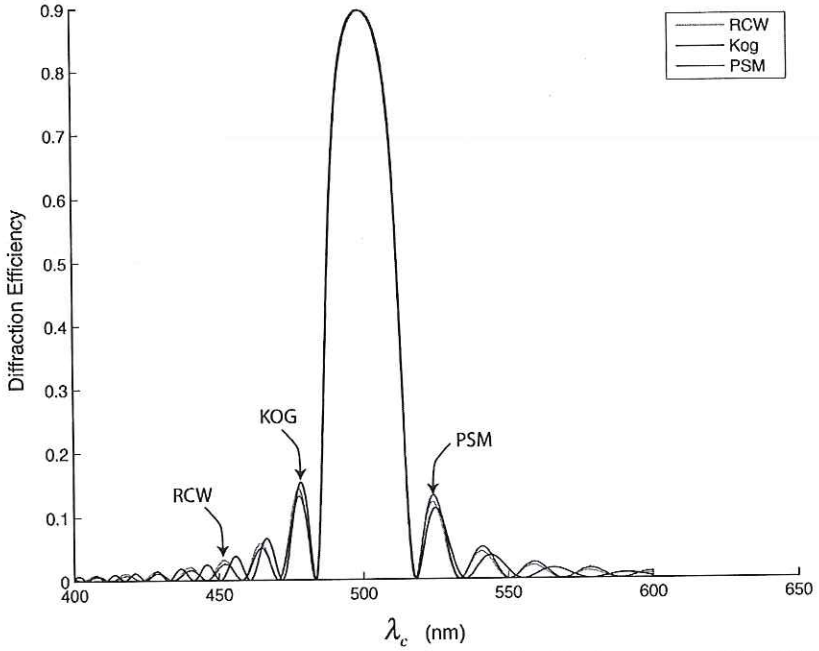

Fig.2 Comparison of the diffraction efficiencies (σ-polarization) predicted by (harmonic permittivity) RCW theory (red), PSM (blue) and Kogelnik (black) for a lossless reflection phase grating having a modulation of n_1/n_0=0.03. The 6 micron deep grating was recorded at λ_r=500nm with reference beams at incidence angles to the grating substrate normal of Φ_r=10° and Φ_o=-25° giving a grating slant of ψ=7.5°. The grating was replayed at an incidence angle of Φ_c=-25°. n_0=1.5.

3.1 Reflection Gratings

3.1.1 Fixed Geometry & Differing Wavelength

Fig.2 shows a comparison of the diffraction efficiencies calculated from the Kogelnik, PSM and RCW models for a typical reflection grating, recorded at one wavelength and replayed at another. The recording and replay geometry is identical here. The graph only shows the l=+1 mode in the RCW calculation as all other modes are negligible. Note that the actual RCW calculation retains 7 modes in total.

Clearly all three theories are quite close. The most obvious observation one can make from Fig.2 is that the characteristic sideband structure of the RCW calculation is clearly best described by the PSM model. This is a pattern observable over many similar graphs. However, in some cases, it appears that the main zeroth order response lobe may perhaps be marginally better described by Kogelnik's theory.

In order to try to characterize the performance of the Kogelnik and PSM theories in a more consistent manner we define the following normalized correlation measures

$$\Gamma_{KOG} = \frac{\int_{\lambda_1}^{\lambda_2} \eta_{KOG}\, \eta_{RCW}\, d\lambda_c}{\sqrt{\int_{\lambda_1}^{\lambda_2} \eta_{KOG}^2 d\lambda_c \int_{\lambda_1}^{\lambda_2} \eta_{RCW}^2\, d\lambda_c}} \quad ; \quad \Gamma_{PSM} = \frac{\int_{\lambda_1}^{\lambda_2} \eta_{PSM}\, \eta_{RCW} d\lambda_c}{\sqrt{\int_{\lambda_1}^{\lambda_2} \eta_{PSM}^2\, d\lambda_c \int_{\lambda_1}^{\lambda_2} \eta_{RCW}^2\, d\lambda_c}} \tag{14}$$

These measures give a value of 1 for a perfect match to l=+1 RCW theory. The great advantage of using such measures is that we may examine many tens of thousands of cases and identify patterns both dispassionately and with relative ease. Fig.3 shows a series of graphs showing the measures of equations (14) plotted versus all possible recording incidence

angles and grating slants. The graphs pertain to a grating of 8μm thickness recorded at λ_r=500nm and having a modulation of n_1/n_0=0.03. The integration is carried out from 400nm to 600nm.Clearly the PSM model appears slightly but consistently closer to the RCW calculation for these gratings. In order to study how this behavior changes for different grating thicknesses and different grating modulations we plot in Fig.4 a surface contour plot of the quantity

$$\Theta(d; n_1/n_0) = \frac{1}{\Phi_{c2} - \Phi_{c1}} \int_{\Phi_c=\Phi_{c1}=-40^\circ}^{\Phi_c=\Phi_{c2}=40^\circ} (\Gamma_{PSM}(\Phi_c) - \Gamma_{KOG}(\Phi_c)) d\Phi_c \qquad (15)$$

for the case of an internal incidence object beam recording beam angle of Φ_o=-30°(with respect to the substrate normal). Graphs for all possible different object recording angles look

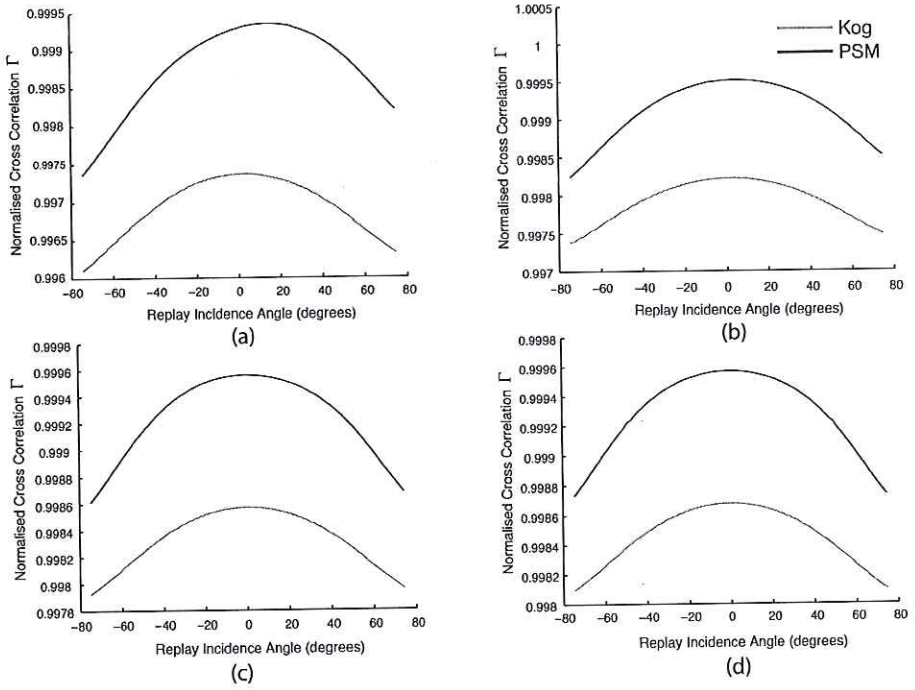

Fig.3 Normalized cross-correlation functions (equations 14) for a comparison of Kogelnik versus (harmonic permittivity) RCW theory and PSM versus (harmonic permittivity) RCW theory (σ-polarization). The graphs pertain to a grating of 8 microns thickness and having a modulation of n_1/n_0=0.03. Graphs (a)-(d) show different internal object beam recording incidence angles with respect to the grating substrate normal. (a) Φ_o=-40° (b) Φ_o=-27°, (c) Φ_o=-14°, (d) Φ_o=0°. The x-axis represents the external incidence replay angle with respect to the grating substrate normal, Φ_c which is equal to the reference recording angle, Φ_r. Grating recorded at λ_r=500nm. n_0=1.5

almost identical. Graphs for different visible wavelengths are also very similar.

We therefore come to the general conclusion that for gratings in the range zero to 10 microns having a modulation n_1/n_0 between zero and 0.06, the PSM model produces a slightly closer estimation than Kogelnik's theory of diffractive efficiency to the RCW calculation for any possible grating in terms of Γ. Further graphs show that this picture continues to larger grating thickness with PSM consistently producing a better estimation as long as the modulation is not too high. This range covers essentially all gratings in visual imaging holography and a sizeable segment of optical element holography.

For extremely thin gratings and for very highly modulated gratings, the situation appears however to reverse and here Kogelnik's model now seems to produce a better match to RCW

theory. As an example Fig.5 shows a highly modulated grating where Kogelnik's theory clearly appears to provide the better estimate of diffraction efficiency. However it must be remembered that the standard RCW calculation describes a grating of harmonic permittivity whereas PSM describes a grating of harmonic index. Accordingly it is not at all surprising that we observe that Kogelnik's theory starts to agree better with standard RCW theory at high modulation. In the appendix we discuss how the RCW calculation may be modified to describe a harmonic index profile. When the calculation is rerun for Fig.5 with the appropriate modifications the PSM diffraction estimate improves substantially, showing that it is actually now slightly closer to the harmonic index RCW calculation than Kogelnik's estimate.

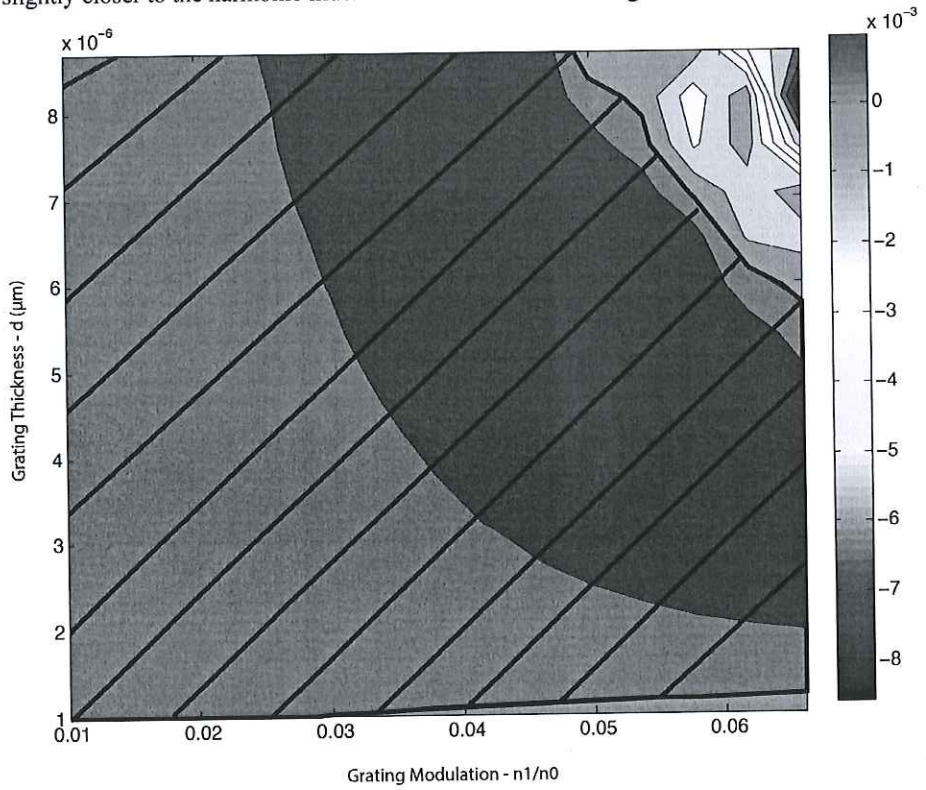

Fig.4. Surface contour plot of the normalized cross-correlation measure defined in equation 15 for the case of an internal object beam recording angle of Φ_o=-30° (σ-polarization). The hashed area represents the region where the correlation measure is positive indicating that the PSM theory is to be preferred here. The large (blue) negative feature in the top right-hand corner is due to the rapidly rising difference between harmonic-index RCW theory and harmonic-permittivity RCW theory as discussed in the text.

The normalized correlation measure, Γ provides an impartial method of assessing the performance of the PSM and Kogelnik theories. Nonetheless it should be pointed out that it represents an average over the whole spectral curve. As such certain features of the spectral response (for example sideband structure or main lobe form) may actually be represented better by the theory having a smaller value of Γ if these features are disproportionately outweighed by other features of opposite correlation.

3.1.2. Fixed Wavelength and Differing Geometry

In the previous section we examined how reflection gratings which were recorded and replayed with a fixed geometry, behaved when illuminated by differing wavelengths. For completeness we now examine the case of fixing the wavelength and varying the replay

reference angle in relation to the recording angle. Fig.6 shows a typical fixed wavelength plot of diffractive efficiency versus replay angle. For this case we see a rather better duplication of the RCW result by the PSM theory as opposed to Kogelnik's theory. However this is not always the case and in order to try and understand which analytic theory is to be preferred under what circumstances we again make use of a normalized correlation measure

$$\Gamma_{KOG} = \frac{\int_{\Phi_1}^{\Phi_2} \eta_{KOG}\,\eta_{RCW}\,d\Phi_c}{\sqrt{\int_{\Phi_1}^{\Phi_2} \eta_{KOG}^2\,d\Phi_c \int_{\Phi_1}^{\Phi_2} \eta_{RCW}^2\,d\Phi_c}} \quad ; \quad \Gamma_{PSM} = \frac{\int_{\Phi_1}^{\Phi_2} \eta_{PSM}\,\eta_{RCW}\,d\Phi_c}{\sqrt{\int_{\Phi_1}^{\Phi_2} \eta_{PSM}^2\,d\Phi_c \int_{\Phi_1}^{\Phi_2} \eta_{RCW}^2\,d\Phi_c}} \tag{16}$$

where the integration in equation (14) over replay wavelength has now been replaced by an integration over incidence replay angle. Fig.7 shows a series of graphs showing the measures of equations (16) plotted versus all possible recording incidence angles and grating slants. The graphs pertain to a grating thickness of 8μm, a recording wavelength of λ_r=500nm and a

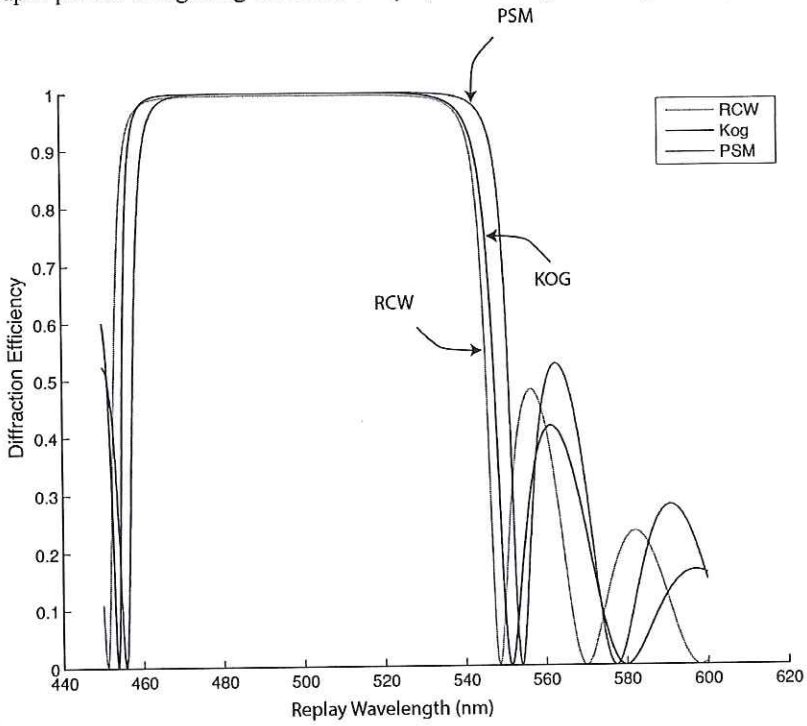

Fig.5 Example of a rather extreme case (σ-polarization) in which there is a clearly saturated broadband response in a relatively thin reflection grating. Here Kogelnik's theory appears closer to RCW theory than PSM only because the RCW calculation used here models a harmonic permittivity profile rather than a harmonic index profile. The grating modulation is n1/n0=0.15 and the grating thickness is 3 microns. Recording wavelength λ_r=500nm. Grating recorded using internal object beam of Φ_o=-20° and internal reference beam Φ_r=-35°. Recording and replay geometries are the same. n_0=1.5.

modulation of n_1/n_0=0.03. The integration is carried out from -40° to 40° internal replay incidence angle. As with the corresponding case of Fig.3, the PSM model appears slightly but consistently closer to the standard (harmonic permittivity) RCW calculation.

As before, in order to study how this behavior changes for different grating thicknesses and different grating modulations we plot in Fig.8 a surface contour plot of the quantity

$$\Theta(d;n_1/n_0)=\frac{1}{\Phi_{r2}-\Phi_{r1}}\int_{\Phi_r=\Phi_{r1}=-40^\circ}^{\Phi_r=\Phi_{r2}=40^\circ}(\Gamma_{PSM}(\Phi_r)-\Gamma_{KOG}(\Phi_r))d\Phi_r \qquad (17)$$

for the case of an internal incidence object beam recording beam angle of Φ_o=-30° (with respect to the substrate normal). This graph appears extremely similar to Fig. 4. In addition graphs for all possible different object recording angles and other visible wavelengths also look very similar. The present angle dependent study therefore simply substantiates the picture we observe with the wavelength study above: for gratings in the range zero to 10

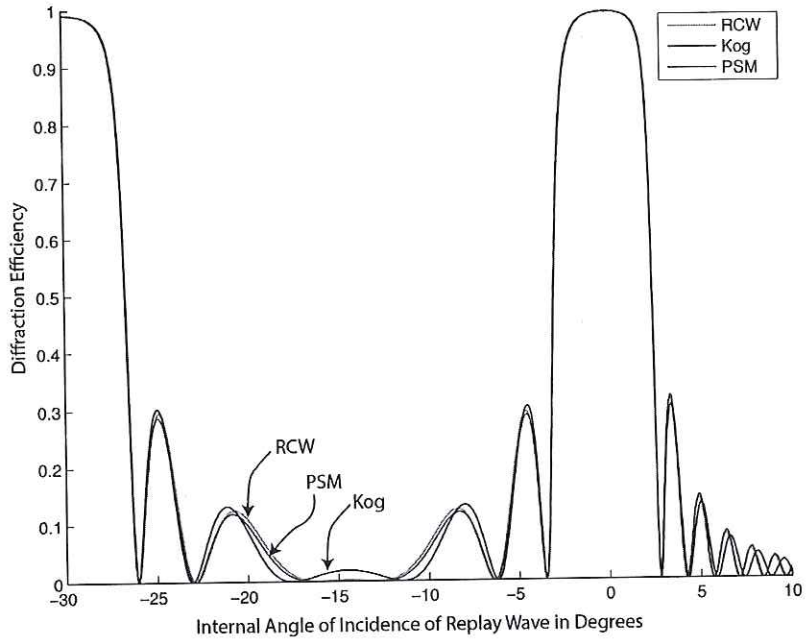

Fig.6 Typical graph showing diffraction efficiency (σ-polarization) as predicted by (harmonic-permittivity) RCW theory (l=+1 mode), PSM and Kogelnik, against internal replay incidence angle with respect to the substrate normal for the fixed geometry case. The grating is 15 microns thick and has a modulation of n_1/n_0=0.02. It was recorded and replayed at λ_r=500nm. Reference recording beam angles were Φ_o=0 and Φ_r=-30° (internal). n_0=1.5. The RCW calculation retained 7 modes.

microns having a modulation n_1/n_0 between zero and 0.06, the PSM model produces a slightly closer estimation than Kogelnik's theory of diffractive efficiency to the standard RCW calculation for any possible grating in terms of Γ. For very high modulation, as in the wavelength study, account must be taken of the fact that PSM describes a harmonic index grating rather than a harmonic permittivity grating; this remains the major reason for the apparent dominance of Kogelnik's theory observable in the upper right-hand corner of Fig.8.

3.2 Transmission Gratings

3.2.1 Fixed geometry and Differing Wavelength

Figs.9 and 10 show comparisons of the diffraction efficiencies calculated from the Kogelnik, PSM and standard (harmonic permittivity) RCW models for typical transmission gratings with zero slant which have been recorded at one wavelength and replayed at another. The recording and replay geometry is identical. The graphs only show the l=+1 mode in the RCW case although as previously 7 modes have been retained in the calculation.

Clearly the picture is rather different here from that of the reflection case. Although there is good agreement between PSM, Kogelnik and RCW theory for small modulations and large incidence angle with respect to the grating substrate normal, as the modulation increases or the angle increases (leading to an effectively smaller incidence angle with respect to the grating substrate) then the difference between the Kogelnik and PSM theories becomes significant. And it is clear that Kogelnik's theory is substantially closer to the RCW calculation under these conditions. In addition the side-band structure, which PSM virtually always predicts better in the reflection case, is seen here to be predicted better by Kogelnik's theory. Fig.11 shows similar graphs for various gratings with a slant angle of 70 degrees. We see that slant does not substantially alter the above picture. In addition, changing the RCW algorithm to model a harmonic index does not change the picture, even at high modulation.

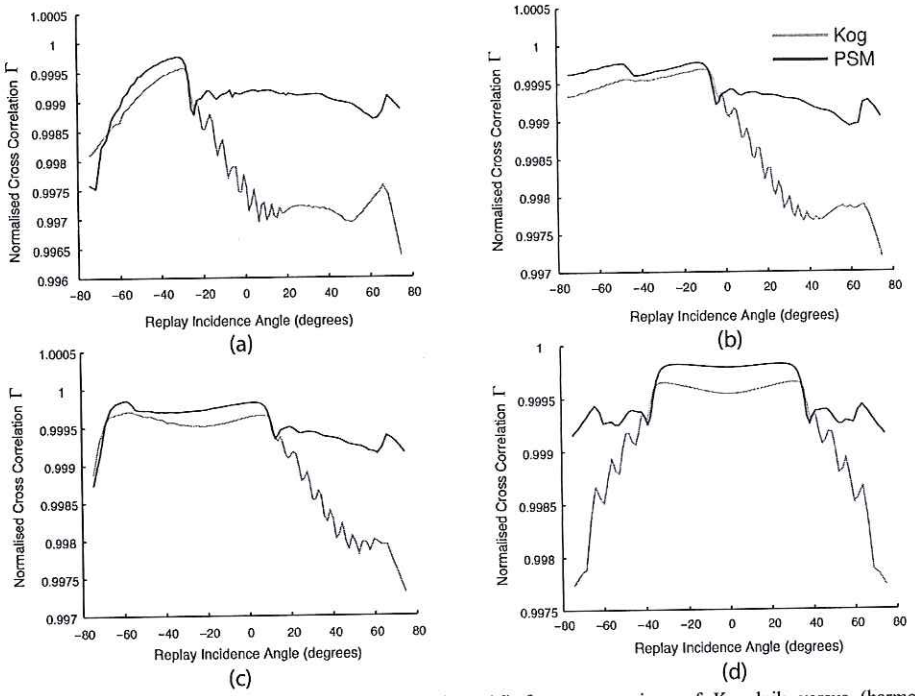

Fig.7 Normalized cross-correlation functions (equations 16) for a comparison of Kogelnik versus (harmonic permittivity) RCW theory and PSM versus (harmonic permittivity) RCW theory (σ-polarization). The graphs pertain to a grating of 8 microns thickness and having a modulation of n_1/n_0=0.03. Graphs (a)-(d) show different internal object beam recording incidence angles with respect to the grating normal. (a) Φ_o =-40°, (b) Φ_o =-27°, (c) Φ_o =-14° and (d) Φ_o =0°. The x-axis represents the external incidence recording angle with respect to the grating normal. Grating recorded at λ_r=500nm. n_0=1.5.

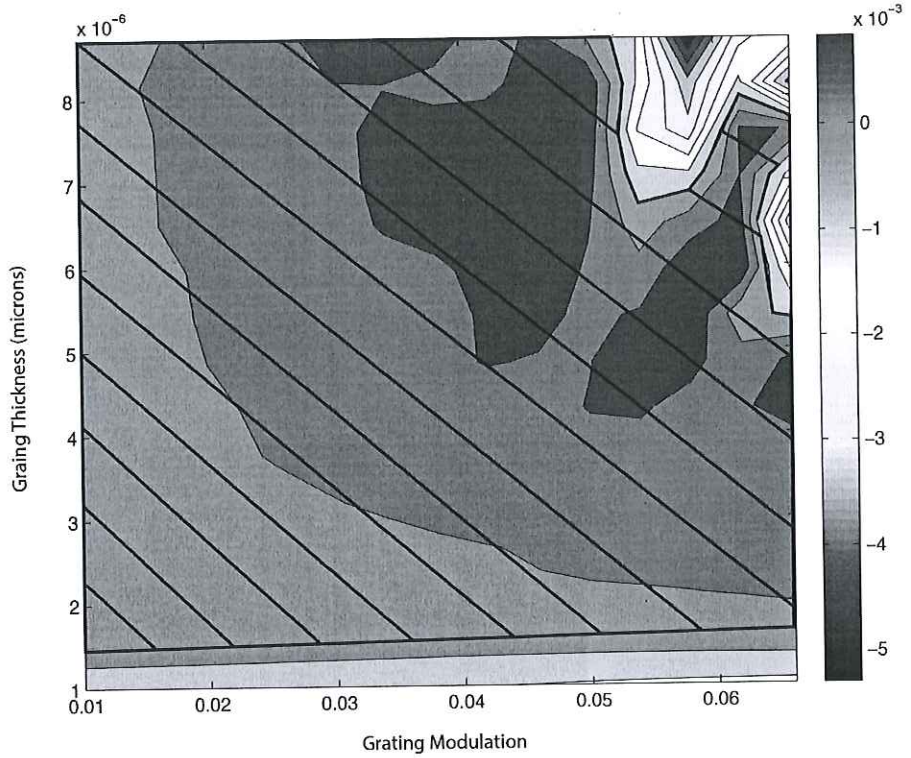

Fig.8 Surface contour plot of the normalized cross-correlation measure defined in equation 17 for the case of an internal object beam recording angle of Φ_o=-30° (σ-polarization). The hashed area represents the region where the correlation measure is positive indicating that the PSM theory is to be preferred here. As in Fig.4 the large (blue) negative feature in the top right-hand corner is due to the rapidly rising difference between harmonic-index RCW theory and harmonic-permittivity RCW theory as discussed in the text.

Kogelnik's theory clearly provides a somewhat better picture of diffraction in the transmission case. This picture is substantiated for many different possible parameters. Unlike the reflection case, where often Kogelnik's theory and PSM produce extremely close results, the differences observable by the naked eye in the transmission case clearly obviate the necessity of a correlation analysis. Nevertheless whilst in the transmission case it is clear that Kogelnik's theory almost always produces the closest results to RCW theory, an important observation is that PSM does produce a relatively good description of diffraction in the transmission grating.

3.2.2 Fixed Wavelength and Differing Geometry

Fig.12 shows some examples of transmission gratings recorded and replayed at different angles. A detailed comparison of many different parameters yields the same picture as observed in the previous section. Although the PSM and Kogelnik theories produce close results for small modulation and smaller incidence angles with respect to the grating plane normal, in many "usual" transmission gratings there is a clear difference between the two theories with Kogelnik's theory providing the better estimation of diffractive efficiency.

4 Discussion

The major conclusion of the present work is that the PSM model provides a slightly better estimation of diffractive efficiency for a wide variety of planar reflection holographic gratings than that provided by Kogelnik's model. This wide variety comprises all of optical imaging

holography and a significant proportion of optical element holography. Nevertheless, despite PSM agreeing exactly with the Kogelnik model at Bragg resonance, Kogelnik's theory almost always provides the better estimate for the transmission grating.

That the PSM theory prevails over Kogelnik's theory, albeit in a relatively minor way over such a large range of reflection gratings, can at first sight appear rather perplexing. Kogelnik's theory, after all, can be derived trivially from the rigorous coupled wave equations (25) by simply dropping the second order derivatives and retaining only the l=+1 (or S) mode and the l=0 or R mode. This procedure immediately yields Kogelnik's equations.

Both Kogelnik's equations and the PSM equations consist of a pair of extremely similar first order coupled differential equations with identical boundary conditions. Had the second order derivatives been kept in the derivation of Kogelnik's equations we would have arrived (in the case of zero slant) at Kong's second order set[11] with rather different boundary conditions. One could therefore be forgiven for assuming that the PSM model had also effectively neglected second order derivatives. However this is not the case as the PSM model makes use of the Fresnel propagation coefficients that are derived from plane wave solutions of Maxwell's equations and these manifestly include the second order derivatives.

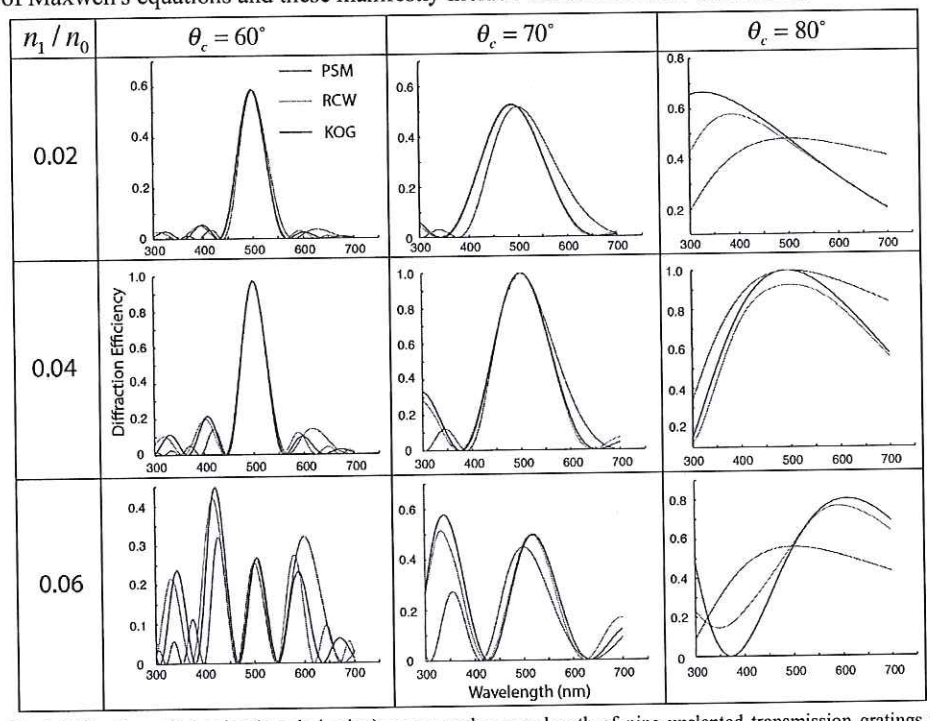

Fig.9 Diffractive efficiencies (σ-polarization) versus replay wavelength of nine unslanted transmission gratings of thickness 4 microns. The graphs cover three (internal) incidence angles with respect to the grating plane normal and three modulations. All gratings were recorded and replayed at the same angle. Recording wavelength was λ_r=500nm. n_0=1.5. (Harmonic permittivity) RCW theory: red, Kogelnik Model: black and PSM Model: blue.

The PSM model therefore contains an implicit modification due to the second order derivatives present in RCW theory. That this is so is also evident by a consideration of the unslanted grating where the governing PSM equations can be shown to represent an exact solution of Maxwell's equations[1,4] - showing again that the second order derivatives have been essentially correctly retained in this limit.

Another major reason that the PSM model provides such a good description of reflective holographic gratings is Snell's law. This law greatly restricts the possible slant angles in reflection gratings and the possible incidence angles of the illumination and image waves. As

we have pointed out above, the governing PSM equations represent an exact solution of Maxwell's equations for the unslanted reflection grating[1,4]. In this case the S wave of PSM is given by the infinite sum of all reflected waves in RCW theory. However, in order to solve these PSM equations analytically one is forced to assume a constant propagation direction. The error in this assumption is effectively zero at normal incidence and grows with incidence angle. However due to the limitation of incidence angle by Snell's law, the approximation of a constant wave propagation direction is rather good.

Finally, grating slant plays a role in understanding PSM. But in the reflection grating, the slant angle is greatly limited by Snell's law. The PSM model is based on an infinite sum of Fresnel waves. And these Fresnel waves are plane wave solutions of Maxwell's equations and such solutions are exact only for infinitely long grating planes. This is indeed the case for the unslanted reflection grating. However as soon as one introduces slant into the grating, each fringe plane becomes finite. Notwithstanding this, given the slant angles possible under Snell's

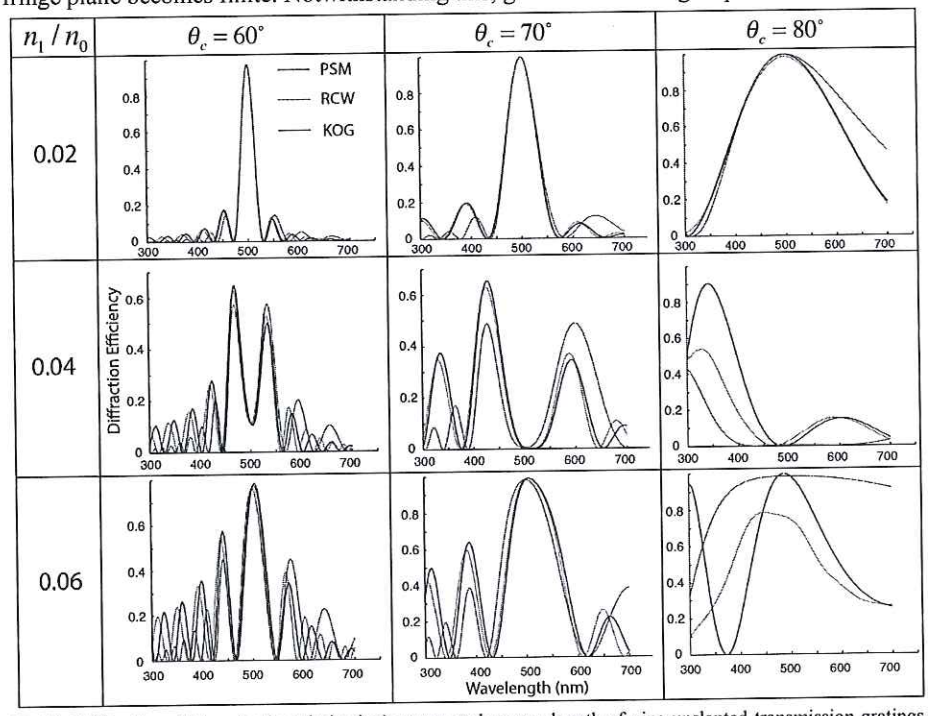

Fig.10. Diffractive efficiencies (σ-polarization) versus replay wavelength of nine unslanted transmission gratings of thickness 8 microns. The graphs cover three (internal) incidence angles with respect to the grating plane normal and three modulations. All gratings were recorded and replayed at the same angle. Recording wavelength was λ_r=500nm. n_0=1.5. (Harmonic Permittivity) RCW theory: red, Kogelnik Model: black and PSM Model: blue.

law, the grating planes are always relatively long compared to the wavelength for usual optical reflection gratings. Accordingly it is not surprising that grating tilt actually has a rather limited effect on the PSM estimations of diffraction efficiency in the reflection geometry.

PSM is a theory that naturally describes a harmonic index profile whereas both Kogelnik's theory and standard RCW theory describe a harmonic permittivity profile. This difference arises because both Kogelnik's model and standard RCW theory seek to solve the Helmholtz equation within the grating in a direct manner and this equation is explicitly linear in permittivity. In contrast, the differential representation of the PSM model is essentially linear in the index rather than in permittivity. As such PSM produces a unique analytical form for the diffraction efficiency of a harmonic index grating whereas Kogelnik's model produces

a unique analytic form relating to a harmonic permittivity grating. For small index, or equivalently for small permittivity, there is therefore essentially no difference in the gratings that PSM, RCW theory and Kogelnik's theory describe. However at high index PSM describes a slightly different grating. This means that in order to rigorously compare the PSM model against RCW theory at high index a variant of RCW theory must be employed. This variant is described in the appendix and has been used to check all the results presented here.

The main difference we see in using a harmonic index version of RCW theory is in the case of high index reflection gratings. In particular we no longer observe that Kogelnik's theory starts to provide the better estimate of diffraction efficiency above an index modulation of n1/n0=0.06. Rather PSM continues now to provide the closer estimate to (the harmonic index) RCW theory.

Most of the above arguments may be applied to the transmission grating to understand why the PSM theory provides a clearly worse description of diffraction than Kogelnik's theory here. We should perhaps clarify the word "worst". In many cases PSM provides a prediction of the diffractive efficiency that is actually extremely close to Kogelnik's prediction. But the accuracy offered by PSM is on average substantially worse than the exceptional accuracy this same theory manifests in the reflection regime.

Comparing PSM and Kogelnik's theories of the transmission grating against harmonic index RCW theory as opposed to harmonic permittivity RCW theory does not change the general conclusion.

The greatest problem for PSM and the transmission grating is the intrinsic grating slant. In the transmission grating Snell's law conspires to produce illumination incidence angles with respect to the grating plane of between 50 and 90 degrees. These are extremely large angles

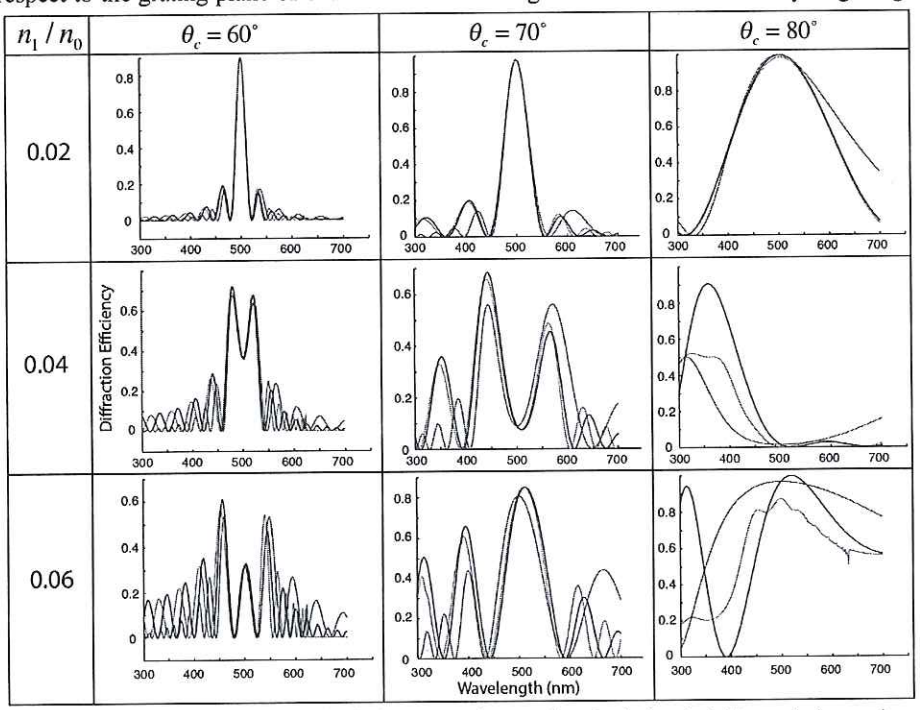

Fig.11. Diffractive efficiencies (σ-polarization) versus replay wavelength of nine slanted transmission gratings of thickness 8 microns and slant angle 70°. The graphs cover three incidence (internal) angles with respect to the grating plane normal and three modulations. All gratings were recorded and replayed at the same angle. Recording wavelength was λ_r=500nm. n_0=1.5. (Harmonic Permittivity) RCW theory: red, Kogelnik Model: black and PSM Model: blue.

for PSM. Firstly the assumption of a constant propagation direction is now no longer very good; and this is particularly so at high modulation as can be seen by considering Snell's law. But in addition the fringe planes are greatly shortened as compared to the reflection case.

We should also point out that at zero grating slant and very small incidence angle with respect to the substrate plane, Kogelnik's theory does not produce an accurate result as this is the Raman Nath regime which requires a plurality of modes to correctly describe it under RCW theory. In addition it is possible to consider transmission gratings that are only recordable and replayable using index matching techniques. These gratings are characterized by a small incidence angle with respect to the normal of the grating plane. Here PSM and Kogelnik both produce nearly identical predictions. However both are wrong, as again high order modes are required for a proper description of this regime.

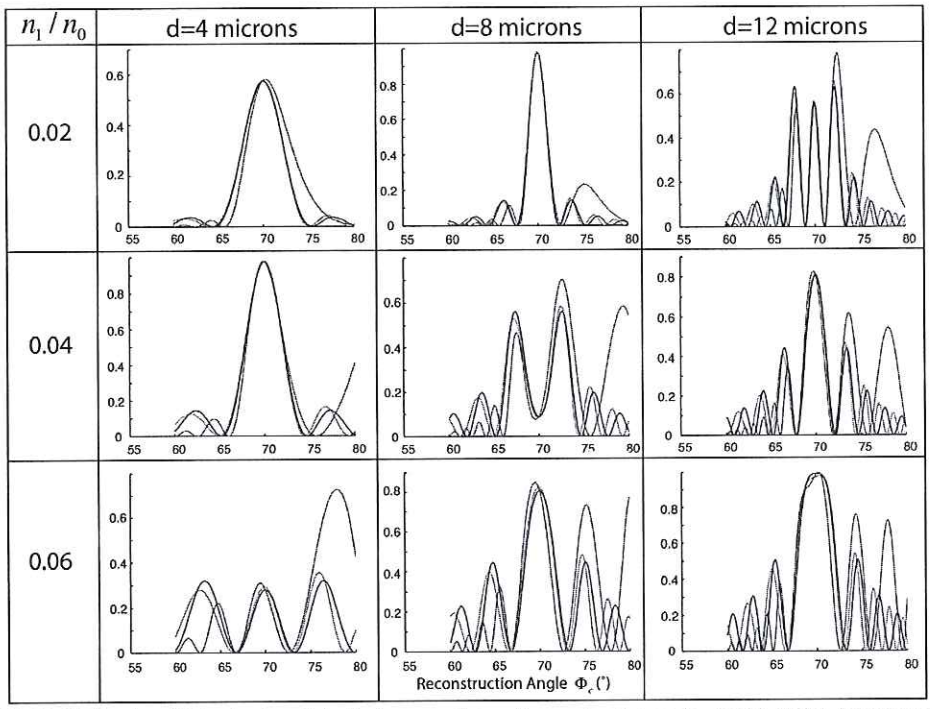

Fig.12. Diffractive efficiencies (σ-polarization) versus (internal) reconstruction angle of nine slanted transmission gratings having a slant angle of 70°. The graphs cover three grating thicknesses and three modulations. All gratings were recorded at 70° (internal angle) with respect to the grating plane normal and replayed at an angle between 60° and 80° (internal angles). Recording wavelength was λ_r=500nm. n_0=1.5. (Harmonic Permittivity) RCW theory: red, Kogelnik Model: black and PSM Model: blue.

5 Conclusion

Calculated diffractive efficiencies in the visible spectral band from lossless planar holographic phase gratings have been studied using the PSM and Kogelnik models of diffraction for the case of the σ-polarization. The results have been numerically compared with rigorous coupled wave calculations over a wide parameter space covering both transmission and reflection geometries. For the great majority of reflection gratings, the PSM model has been shown to consistently provide a slightly superior estimation of the diffractive efficiency. This is particularly evident in a clearly superior description of the diffractive sideband structure (either in terms of wavelength or angle) for most gratings. For the transmission grating, however, Kogelnik's theory has been shown to provide both a somewhat superior estimation of diffractive efficiency in general and a clearly superior description of the diffractive side-band structure.

6 Appendix: Rigorous Coupled Wave Theory

6.1 Standard RCW Theory

Rigorous coupled wave theory was first described by Moharam and Gaylord[10]. Here we follow the approach outlined in appendix 8 of Bjelkhagen and Brotherton-Ratcliffe[4]. For the lossless planar grating with isotropic permittivity under illumination with the σ-polarization the Helmholtz equation may be written

$$\frac{\partial^2 u}{\partial x^2}+\frac{\partial^2 u}{\partial y^2}-\gamma^2 u=0 \tag{18}$$

where u is the transverse (z) electric field and the parameter

$$\gamma^2=-\beta^2-2\beta\kappa\left\{e^{i\mathbf{K}\cdot\mathbf{r}}+e^{-i\mathbf{K}\cdot\mathbf{r}}\right\} \tag{19}$$

defines the harmonic permittivity distribution within the sinusoidal grating. Following the notation established above, we now consider the case of illumination of the grating by a wave of the form

$$u(y<0)=e^{i(k_x x+k_y y)} \tag{20}$$

where

$$\begin{aligned} k_x &= \beta\sin(\theta_c-\psi)=\beta\sin(\Phi_c)\\ k_y &= \beta\cos(\theta_c-\psi)=\beta\cos(\Phi_c) \end{aligned} \tag{21}$$

In both the front region (y<0) and the rear region (y>d) the average index is assumed to be n_0. Now the Helmholtz field, u(x,y) may be consistently expanded in the following way:

$$u(x,y)=\sum_{l=-\infty}^{\infty}u_l(y)e^{i(k_x+lK_x)x} \tag{22}$$

This expression may be substituted into (18) and (19). On taking the Fourier transform and applying orthogonality we then arrive at the following rigorous coupled wave equations:

$$\left\{(k_x+lK_x)^2-\beta^2\right\}u_l(y)-\frac{d^2u_l}{dy^2}(y)=2\beta\kappa\left\{u_{l-1}(y)e^{iK_y y}+u_{l+1}(y)e^{-iK_y y}\right\} \tag{23}$$

For the case of the simple sinusoidal grating, the transformation

$$u_l(y)=\hat{u}_l(y)e^{i(k_y+lK_y)y} \tag{24}$$

now reduces (23) to the more usual form

$$\begin{aligned} &\frac{d^2\hat{u}_l(y)}{dy^2}+2i(k_y+lK_y)\frac{d\hat{u}_l(y)}{dy}=\\ &\left\{(k_x+lK_x)^2+(k_y+lK_y)^2-\beta^2\right\}\hat{u}_l(y)-2\beta\kappa\left\{\hat{u}_{l-1}(y)+\hat{u}_{l+1}(y)\right\} \end{aligned} \tag{25}$$

used by Moharam and Gaylord[10].

6.2 Harmonic Index RCW Theory

If we are to treat a harmonic index profile as opposed to a harmonic permittivity profile the γ^2 parameter of (19) needs to be changed to the following form

$$\begin{aligned} \gamma^2 &= -\beta^2\left(1+\frac{n_1}{2n_0}\left[e^{i\mathbf{K}\cdot\mathbf{r}}+e^{-i\mathbf{K}\cdot\mathbf{r}}\right]\right)^2\\ &= -(\beta^2+2\kappa^2)-2\beta\kappa\left[e^{i\mathbf{K}\cdot\mathbf{r}}+e^{-i\mathbf{K}\cdot\mathbf{r}}\right]-\kappa^2\left[e^{2i\mathbf{K}\cdot\mathbf{r}}+e^{-2i\mathbf{K}\cdot\mathbf{r}}\right] \end{aligned} \tag{26}$$

We may now proceed as with the standard derivation of RCW theory by letting once again

$$u(x,y)=\sum_{l=-\infty}^{\infty}u_l(y)e^{i(k_x+lK_x)x} \tag{27}$$

Then the Helmholtz equation becomes

$$\begin{aligned}&\left\{(k_x+lK_x)^2-(\beta^2+2\kappa^2)\right\}u_l(y)-\frac{d^2u_l}{dy^2}(y)=\\&2\beta\kappa\left\{u_{l-1}(y)e^{iK_y y}+u_{l+1}(y)e^{-iK_y y}\right\}+\kappa^2\left\{u_{l-2}(y)e^{2iK_y y}+u_{l+2}(y)e^{-2iK_y y}\right\}\end{aligned} \tag{28}$$

Now if we take

$$u_l(y)=\hat{u}_l(y)e^{i(k_y+lK_y)y} \tag{29}$$

we arrive at the appropriate *harmonic index* RCW equation

$$\begin{aligned}&\frac{d^2\hat{u}_l(y)}{dy^2}+2i(k_y+lK_y)\frac{d\hat{u}_l(y)}{dy}=\left\{(k_x+lK_x)^2+(k_y+lK_y)^2-(\beta^2+2\kappa^2)\right\}\hat{u}_l(y)\\&-2\beta\kappa\left\{\hat{u}_{l-1}(y)+\hat{u}_{l+1}(y)\right\}-\kappa^2\left\{\hat{u}_{l-2}(y)+\hat{u}_{l+2}(y)\right\}\end{aligned} \tag{30}$$

6.3 Boundary Conditions

Outside the grating equation (25) and (30) simplify to

$$\frac{d^2\hat{u}_l}{dy^2}+2i(k_y+lK_y)\frac{d\hat{u}_l}{dy}-\left\{(k_x+lK_x)^2+(k_y+lK_y)^2-\beta^2\right\}\hat{u}_l=0 \tag{31}$$

The general solution of this differential equation is then

$$\hat{u}_l=A_l e^{-i(k_y+lK_y)y+i\sqrt{\left\{\beta^2-(k_x+lK_x)^2\right\}}y}+B_l e^{-i(k_y+lK_y)y-i\sqrt{\left\{\beta^2-(k_x+lK_x)^2\right\}}y} \tag{32}$$

And so the general solution to the Helmholtz equation in front of the grating is given by

$$\begin{aligned}u(x,y)&=e^{i\sqrt{\left\{\beta^2-k_x^2\right\}}y}e^{ik_x}+\sum_{l=-\infty}^{+\infty}\hat{u}_l e^{-i(k_y+lK_y)y-i\sqrt{\left\{\beta^2-(k_x+lK_x)^2\right\}}y}e^{i(k_x+lK_x)x}e^{i(k_y+lK_y)y}\\&=e^{i\sqrt{\left\{\beta^2-k_x^2\right\}}y}e^{ik_x}+\sum_{l=-\infty}^{+\infty}\hat{u}_l e^{-i\sqrt{\left\{\beta^2-(k_x+lK_x)^2\right\}}y}e^{i(k_x+lK_x)x}\end{aligned} \tag{33}$$

6.3.1 Front Boundary

Continuity of the tangential electric field at the front boundary gives

$$u(x,y=0)=e^{ik_x}+\sum_{l=-\infty}^{+\infty}\hat{u}_l e^{i(k_x+lK_x)x} \tag{34}$$

Likewise the continuity of the tangential magnetic field gives

$$u(x,y=0)'=i\sqrt{\beta^2-k_x^2}e^{ik_x}-i\sum_{-\infty}^{+\infty}(\sqrt{\beta^2-(k_x+lK_x)^2})\hat{u}_l e^{i(k_x+lK_x)x} \tag{35}$$

In both these expressions the left hand side is the field inside the grating and the right hand side is the outside field. Using equation (22) we can rewrite the left hand side of both equations in the following way

$$u(x,y=0)=\sum_{l=-\infty}^{\infty}\hat{u}_l(y=0;i)e^{i(k_x+lK_x)}=e^{ik_x}+\sum_{l=-\infty}^{+\infty}\hat{u}_l(y=0;o)e^{i(k_x+lK_x)x} \tag{36}$$

$$u(x,y=0)' = \sum_{l=-\infty}^{\infty}\left\{ i(k_y + lK_y)\hat{u}_l(y=0;i) + \hat{u}_l{}'(y=0;i)\right\} e^{i(k_x+lK_x)} \\ = i\sqrt{\beta^2 - k_x^2}\, e^{ik_x} - i\sum_{-\infty}^{+\infty}(\sqrt{\beta^2 - (k_x+lK_x)^2})\hat{u}_l(y=0;o)e^{i(k_x+lK_x)x} \tag{37}$$

where "i" means inside the grating and "o" means outside the grating. Taking the Fourier transform with l=0 and dividing by $e^{ik_x x}$ we get

$$\hat{u}_0(y=0;i) = 1 + \hat{u}_0(y=0;o) \tag{38}$$

$$ik_y\hat{u}_0(y=0;i) + \hat{u}_0{}'(y=0;i) = i\sqrt{\beta^2 - k_x^2} - i(\sqrt{\beta^2 - k_x^2})\hat{u}_0(y=0;o) \tag{39}$$

This then gives the required boundary condition at y=0 for l=0

$$\hat{u}_0{}'(y=0;i) = 2ik_y\left\{1 - \hat{u}_0(y=0;i)\right\} \tag{40}$$

The y=0 finite l boundary condition is likewise

$$\hat{u}_l{}'(y=0;i) + i(k_y + lK_y)\hat{u}_l(y=0;i) = -i\left\{\sqrt{\beta^2 - (k_x+lK_x)^2}\right\}\hat{u}_l(y=0;i) \tag{41}$$

6.3.2 Rear Boundary

The general solution outside the rear surface is

$$u(x,y) = \sum_{l=-\infty}^{+\infty}\hat{u}_l e^{-i(k_y+lK_y)y + i\sqrt{\left\{\beta^2 - (k_x+lK_x)^2\right\}}y + i(k_y+lK_y)y} e^{i(k_x+lK_x)x} \\ = \sum_{l=-\infty}^{+\infty}\hat{u}_l e^{i\sqrt{\left\{\beta^2-(k_x+lK_x)^2\right\}}y} e^{i(k_x+lK_x)x} \tag{42}$$

So the y=d boundary condition for all l is

$$\hat{u}_l{}'(y=d;i) + i(k_y + lK_y)\hat{u}_l(y=d;i) = i\left\{\sqrt{\beta^2 - (k_x+lK_x)^2}\right\}\hat{u}_l(y=d;i) \tag{43}$$

6.4 Numerical Solution

We will now use (25) to deduce a state-space formulation of the problem. Equation (30) may be treated in exactly the same manner with trivial modification.

Following Moharam and Gaylord[10] we rewrite equation (25) in the form

$$\frac{d}{dy}\begin{pmatrix} U_{1,l} \\ U_{2,l} \end{pmatrix} = b\begin{pmatrix} U_{1,l} \\ U_{2,l} \end{pmatrix} \tag{44}$$

where we have defined $U_{1,l} = \hat{u}_l$ and $U_{2,l} = d\hat{u}_l / dy$. In order to illustrate how the equations look in component form we now take the case of N=2 where N is the maximum value of the mode number l. From the N=2 equations it is trivial to see how all higher N equations look.

For N=2,

$$\frac{d}{dy}\begin{pmatrix} U_{1,2} \\ U_{1,1} \\ U_{1,0} \\ U_{1,-1} \\ U_{1,-2} \\ U_{2,2} \\ U_{2,1} \\ U_{2,0} \\ U_{2,-1} \\ U_{2,2} \end{pmatrix} = \begin{pmatrix} 0 & 0 & 0 & 0 & 0 & 1 & 0 & 0 & 0 & 0 \\ 0 & 0 & 0 & 0 & 0 & 0 & 1 & 0 & 0 & 0 \\ 0 & 0 & 0 & 0 & 0 & 0 & 0 & 1 & 0 & 0 \\ 0 & 0 & 0 & 0 & 0 & 0 & 0 & 0 & 1 & 0 \\ 0 & 0 & 0 & 0 & 0 & 0 & 0 & 0 & 0 & 1 \\ b_2 & a & 0 & 0 & 0 & c_2 & 0 & 0 & 0 & 0 \\ a & b_1 & a & 0 & 0 & 0 & c_1 & 0 & 0 & 0 \\ 0 & a & b_0 & a & 0 & 0 & 0 & c_0 & 0 & 0 \\ 0 & 0 & a & b_{-1} & a & 0 & 0 & 0 & c_{-1} & 0 \\ 0 & 0 & 0 & a & b_{-2} & 0 & 0 & 0 & 0 & c_{-2} \end{pmatrix} \begin{pmatrix} U_{1,2} \\ U_{1,1} \\ U_{1,0} \\ U_{1,-1} \\ U_{1,-2} \\ U_{2,2} \\ U_{2,1} \\ U_{2,0} \\ U_{2,-1} \\ U_{2,2} \end{pmatrix} \tag{45}$$

where we have introduced coefficients

$$\begin{aligned} a &= -2\beta\kappa \\ b_l &= (k_x + lK_x)^2 + (k_y + lK_y)^2 - \beta^2 \\ c_l &= -2i(k_y + lK_y) \end{aligned} \tag{46}$$

The solution of this Eigen equation is

$$U_\alpha = \sum_m C_m w_{\alpha m} e^{q_m y} \tag{47}$$

where q_m is the m^{th} eigenvalue and w is the matrix of eigenvectors.

6.4.1 Solution of the Eigen Problem

The general solution of the Eigen problem is given by equation (47). For the N=2 problem we can write this explicitly as

$$\begin{pmatrix} U_1 \\ U_2 \\ U_3 \\ U_4 \\ U_5 \\ U_6 \\ U_7 \\ U_8 \\ U_9 \\ U_{10} \end{pmatrix} = \begin{pmatrix} \hat{u}_2 \\ \hat{u}_1 \\ \hat{u}_0 \\ \hat{u}_{-1} \\ \hat{u}_{-2} \\ \hat{u}'_2 \\ \hat{u}'_1 \\ \hat{u}'_0 \\ \hat{u}'_{-1} \\ \hat{u}'_{-2} \end{pmatrix} = \begin{pmatrix} & & & & & & & & & \\ & & & & & & & & & \\ & & & & & & & & & \\ & & & & & & & & & \\ & & & & & & & & & \\ & & & & & & & & & \\ & & & & & & & & & \\ & & & & & & & & & \\ & & & & & & & & & \\ & & & & & & & & & \end{pmatrix} \quad w_{\alpha m} \quad \begin{pmatrix} C_1 e^{q_1 y} \\ C_2 e^{q_2 y} \\ C_3 e^{q_3 y} \\ C_4 e^{q_4 y} \\ C_5 e^{q_5 y} \\ C_6 e^{q_6 y} \\ C_7 e^{q_7 y} \\ C_8 e^{q_8 y} \\ C_9 e^{q_9 y} \\ C_{10} e^{q_{10} y} \end{pmatrix} \tag{48}$$

Now the boundary conditions may be written as

$$U_8(0)=\sum_{m=1}^{10}C_m w_{8m}=2ik_y(1-U_3(0))=2ik_y(1-\sum_{m=1}^{10}C_m w_{3m}) \tag{49}$$

$$U_6(0)=\sum_{m=1}^{10}C_m w_{6m}=\left\{-i(\sqrt{\beta^2-(k_x+2K_x)^2})-i(k_y+2K_y)\right\}\sum_{m=1}^{10}C_m w_{1m} \tag{50}$$

$$U_7(0)=\sum_{m=1}^{10}C_m w_{7m}=\left\{-i(\sqrt{\beta^2-(k_x+K_x)^2})-i(k_y+K_y)\right\}\sum_{m=1}^{10}C_m w_{2m} \tag{51}$$

$$U_9(0)=\sum_{m=1}^{10}C_m w_{9m}=\left\{-i(\sqrt{\beta^2-(k_x-K_x)^2})-i(k_y-K_y)\right\}\sum_{m=1}^{10}C_m w_{4m} \tag{52}$$

$$U_{10}(0)=\sum_{m=1}^{10}C_m w_{10m}=\left\{-i(\sqrt{\beta^2-(k_x-2K_x)^2})-i(k_y-2K_y)\right\}\sum_{m=1}^{10}C_m w_{5m} \tag{53}$$

$$U_6(d)=\sum_{m=1}^{10}C_m w_{6m}e^{q_m d}=\left\{i(\sqrt{\beta^2-(k_x+2K_x)^2})-i(k_y+2K_y)\right\}\sum_{m=1}^{10}C_m w_{1m}e^{q_m d} \tag{54}$$

$$U_7(d)=\sum_{m=1}^{10}C_m w_{7m}e^{q_m d}=\left\{i(\sqrt{\beta^2-(k_x+K_x)^2})-i(k_y+K_y)\right\}\sum_{m=1}^{10}C_m w_{2m}e^{q_m d} \tag{55}$$

$$U_8(d)=\sum_{m=1}^{10}C_m w_{8m}e^{q_m d}=0 \tag{56}$$

$$U_9(d)=\sum_{m=1}^{10}C_m w_{9m}e^{q_m d}=\left\{i(\sqrt{\beta^2-(k_x-K_x)^2})-i(k_y-K_y)\right\}\sum_{m=1}^{10}C_m w_{4m}e^{q_m d} \tag{57}$$

$$U_{10}(d)=\sum_{m=1}^{10}C_m w_{10m}e^{q_m d}=\left\{i(\sqrt{\beta^2-(k_x-2K_x)^2})-i(k_y-2K_y)\right\}\sum_{m=1}^{10}C_m w_{5m}e^{q_m d} \tag{58}$$

These boundary conditions may in turn be rewritten in matrix form

$$\mathbf{Z}\cdot\mathbf{C}=\mathbf{R}+\mathbf{T}\cdot\mathbf{C} \tag{59}$$

where

$$\mathbf{Z}=\begin{pmatrix} w_{61} & w_{62} & w_{63} & w_{64} & w_{65} & w_{66} & w_{67} & w_{68} & w_{69} & w_{610} \\ w_{71} & w_{72} & w_{73} & w_{74} & w_{75} & w_{76} & w_{77} & w_{78} & w_{79} & w_{719} \\ w_{81} & \cdots & & & & & & & & \\ w_{91} & \cdots & & & & & & & & \\ w_{101} & \cdots & & & & & & & & \\ w_{61}e^{q_1 d} & w_{62}e^{q_2 d} & w_{63}e^{q_3 d} & w_{64}e^{q_4 d} & \cdots & & & & & \\ w_{71}e^{q_1 d} & w_{72}e^{q_2 d} & w_{73}e^{q_3 d} & w_{74}e^{q_4 d} & \cdots & & & & & \\ w_{81} & \cdots & & & & & & & & \\ w_{91} & \cdots & & & & & & & & \\ w_{101} & \cdots & & & & & & & & \end{pmatrix} \tag{60}$$

$$\mathbf{T} = \begin{pmatrix} f_2 w_{11} & f_2 w_{12} & f_2 w_{13} & f_2 w_{14} & f_2 w_{15} & f_2 w_{16} & \cdots \\ f_1 w_{21} & f_1 w_{22} & f_1 w_{23} & f_1 w_{24} & \cdots & & \\ f_0 w_{31} & \cdots & & & & & \\ f_{-1} w_{41} & \cdots & & & & & \\ f_{-2} w_{51} & \cdots & & & & & \\ g_2 w_{11} e^{q_1 d} & g_2 w_{12} e^{q_2 d} & g_2 w_{13} e^{q_3 d} & g_2 w_{14} e^{q_4 d} & g_2 w_{15} e^{q_5 d} & g_2 w_{16} e^{q_6 d} & \cdots \\ g_1 w_{21} e^{q_1 d} & g_1 w_{22} e^{q_2 d} & g_1 w_{23} e^{q_3 d} & g_1 w_{24} e^{q_4 d} & \cdots & & \\ g_0 w_{31} e^{q_1 d} & \cdots & & & & & \\ g_{-1} w_{41} e^{q_1 d} & \cdots & & & & & \\ g_{-2} w_{51} e^{q_1 d} & \cdots & & & & & \end{pmatrix} \tag{61}$$

and

$$\mathbf{R} = \begin{pmatrix} 0 \\ 0 \\ 2ik_y \\ 0 \\ 0 \\ 0 \\ 0 \\ 0 \\ 0 \\ 0 \end{pmatrix} \tag{62}$$

and where

$$\begin{aligned} f_l &= \left\{ -i\sqrt{\beta^2 - (k_x + lK_x)^2} - i(k_y + lK_y) \right\} \\ g_l &= \left\{ i\sqrt{\beta^2 - (k_x + lK_x)^2} - i(k_y + lK_y) \right\} \end{aligned} \tag{63}$$

The matrix equation may now be solved by computing

$$\mathbf{C} = (\mathbf{Z} - \mathbf{T})^{-1}\mathbf{R} \tag{64}$$

The diffraction efficiencies of the transmitted modes are then defined as[4]

$$\eta_{-l}(T) = \frac{\sqrt{\beta^2 - (k_x + lK_x)^2}}{k_y} \hat{u}_l(y = d)\hat{u}_l^*(y = d) \tag{65}$$

Likewise the diffraction efficiencies of the reflected modes are defined as

$$\eta_{-l}(R) = \frac{\sqrt{\beta^2 - (k_x + lK_x)^2}}{k_y} \hat{u}_l(y=0)\hat{u}_l^*(y=0) \quad \forall l \neq 0$$

$$\eta_0(R) = (\hat{u}_l(y=0) - 1)(\hat{u}_l^*(y=0) - 1) \qquad l = 0 \tag{66}$$

Note the change of sign on l, which we have made here in order for the signs of the modes to correspond to the notation used by Moharam[10]. Note also that in the case of *harmonic index* RCW theory one needs only to change equations (45) and (46). These must be replaced by

$$\frac{d}{dy}\begin{pmatrix} U_{1,2} \\ U_{1,1} \\ U_{1,0} \\ U_{1,-1} \\ U_{1,-2} \\ U_{2,2} \\ U_{2,1} \\ U_{2,0} \\ U_{2,-1} \\ U_{2,2} \end{pmatrix} = \begin{pmatrix} 0 & 0 & 0 & 0 & 0 & 1 & 0 & 0 & 0 & 0 \\ 0 & 0 & 0 & 0 & 0 & 0 & 1 & 0 & 0 & 0 \\ 0 & 0 & 0 & 0 & 0 & 0 & 0 & 1 & 0 & 0 \\ 0 & 0 & 0 & 0 & 0 & 0 & 0 & 0 & 1 & 0 \\ 0 & 0 & 0 & 0 & 0 & 0 & 0 & 0 & 0 & 1 \\ b_2 & a & \kappa^2 & 0 & 0 & c_2 & 0 & 0 & 0 & 0 \\ a & b_1 & a & \kappa^2 & 0 & 0 & c_1 & 0 & 0 & 0 \\ \kappa^2 & a & b_0 & a & \kappa^2 & 0 & 0 & c_0 & 0 & 0 \\ 0 & \kappa^2 & a & b_{-1} & a & 0 & 0 & 0 & c_{-1} & 0 \\ 0 & 0 & \kappa^2 & a & b_{-2} & 0 & 0 & 0 & 0 & c_{-2} \end{pmatrix} \begin{pmatrix} U_{1,2} \\ U_{1,1} \\ U_{1,0} \\ U_{1,-1} \\ U_{1,-2} \\ U_{2,2} \\ U_{2,1} \\ U_{2,0} \\ U_{2,-1} \\ U_{2,2} \end{pmatrix} \tag{67}$$

and

$$\begin{aligned} a &= -2\beta\kappa \\ b_l &= (k_x + lK_x)^2 + (k_y + lK_y)^2 - (\beta^2 + 2\kappa^2) \\ c_l &= -2i(k_y + lK_y) \end{aligned} \tag{68}$$